

Gaussian Quantum Metrology with Realistic Linear Sensors

Jacques Ding,^{1,*} James W. Gardner,² Tuvia Gefen,³ and Yanbei Chen⁴

¹*Laboratoire Astroparticule et Cosmologie, Université Paris Cité, CNRS, F-75013 Paris, France*

²*Pritzker School of Molecular Engineering, University of Chicago, Illinois 60637, USA*

³*Racah Institute of Physics, The Hebrew University of Jerusalem, Jerusalem 9190401, Israel*

⁴*Theoretical Astrophysics, Walter Burke Institute for Theoretical Physics, California Institute of Technology, Pasadena, California 91125, USA*

(Dated: June 30, 2026)

Quantum sensing promises enhanced precision, but the usual quantum Cramer Rao bound can be too optimistic for realistic linear sensors, where squeezing, filtering, and loss reshape quantum noise. We derive the tight Holevo Cramer Rao bound and show that realistic degradation yields a hierarchy with the usual bound and homodyne readout. This hierarchy already exists in gravitational-wave detectors. We propose a hardware-efficient readout that reaches the Holevo bound without extra signal loss, increasing compact-binary detection rates by up to 25% over the present LIGO homodyne readout.

Introduction — Linear quantum sensors encode classical input waveforms in continuous-variable quantum output fields. Their sensitivity is set not only by the total quantum noise, but also by how this noise is distributed among conjugate quadratures and sidebands. Gravitational-wave (GW) interferometers are a prominent example: each Fourier component of the strain waveform has two real sine/cosine amplitudes, so the measurement is intrinsically multiparameter.

The commonly quoted Quantum Cramer Rao bound (QCRB) optimizes the readout for each parameter separately. It is therefore a lower bound, but it is physically attainable only when its optimal estimators are compatible. The relevant attainable bound in a multiparameter problem is the Holevo Cramer Rao bound (HCRB), which optimizes over joint measurements. In ideal tuned, lossless models often used for gravitational-wave interferometers, this distinction is invisible: the QCRB, the HCRB, and variational readout – the frequency-dependent homodyne strategy used to evade radiation-pressure backaction – all coincide [1–9]. However, the LIGO and Virgo detectors, starting with the fourth observing run (O4), include frequency-dependent squeezing [10, 11], which comes with optical loss, mismatch, and dephasing [12, 13]. These effects can unbalance the quantum noise distribution over the positive and negative frequency sidebands, so it is no longer evident that the usual QCRB/variational-readout picture gives the attainable quantum limit.

In this Letter, we derive the exact spectral HCRB for tuned Gaussian linear sensors with realistic degradation. We find a hierarchy controlled by the output sideband imbalance: for weak imbalance, the QCRB is already unattainable while variational readout still reaches the HCRB; for strong imbalance, all three bounds separate and the optimum becomes nonprojective (see Table I). We identify the attaining measurements and introduce symplectodyne readout, a narrowband implementation based on local-oscillator modulation rather than addi-

Loss	Imbalance	Hierarchy	Attainability
No	$\Delta = 0$	QCRB = HCRB = Var	PVM
Yes	$\Delta = 0$	QCRB = HCRB = Var	PVM
Yes	$0 < \Delta \leq \frac{1}{2}$	QCRB < HCRB = Var	PVM
Yes	$ \Delta > \frac{1}{2}$	QCRB < HCRB < Var	POVM

TABLE I. Hierarchy between the QCRB, HCRB, and variational readout (Var) for tuned detectors, depending on the presence of loss, whether they create sideband imbalance, and which regime – projective (PVM) or non-projective (POVM) – the optimal measurement belongs to.

tional lossy optics in the signal path. Applied to the true, full LIGO O4 quantum noise budget [10, 14, 15], the hierarchy is already present and leads to measurable astrophysical gains.

Multiparameter estimation in linear sensors — Consider a classical signal (e.g. a GW strain component) $h(t)$, coupled to a sensor (e.g. a GW interferometer). In the linear regime, h can be decomposed along its Fourier components $h[\Omega]$, and it is thus sufficient to focus on the estimation problem at a given sideband frequency Ω . Under the standard input-output formalism for linear time-invariant systems [6, 16–18], the two-photon output quadratures at frequency Ω , written as $x^{\text{out}}[\Omega] = (q^{\text{out}}[\Omega], p^{\text{out}}[\Omega])^T$, are given by

$$x^{\text{out}}[\Omega] = H[\Omega] x^{\text{in}}[\Omega] + \sum_j T_j[\Omega] n_j[\Omega] + \chi[\Omega] h[\Omega]. \quad (1)$$

Here $\chi[\Omega]$ is the signal response, while x^{in} and n_j are the quantum input and loss-port fields respectively. The transfer matrices H and T_j depend on the loss mechanisms [12, 13], but are constrained so that x^{out} obeys the canonical commutation relations [18]. For zero-mean input and loss fields, all quantum fluctuations can be grouped into an output-referred noise δx^{out} , giving

$$x^{\text{out}}[\Omega] = \delta x^{\text{out}}[\Omega] + \chi[\Omega] h[\Omega] \quad (2)$$

We introduce the normalized cosine/sine quadratures θ_1 and θ_2 of the waveform, such that $h(t) =$

$\frac{2}{\sqrt{T}\|\chi\|}[\theta_1 \cos(\Omega t) + \theta_2 \sin(\Omega t)]$ where T is the measurement time. Estimating $h(t)$ is therefore equivalent to simultaneously estimating $\theta = (\theta_1, \theta_2)^\top \in \mathbb{R}^2$. At each Ω , the signal therefore labels a displaced Gaussian state ρ_θ . A readout is a POVM $M(dy)$ such that

$$p_\theta(dy) = \text{tr}[\rho_\theta M(dy)], \quad \int \tilde{\theta}_i(y) p_\theta(dy) = \theta_i.$$

Thus $\tilde{\theta}_i$ are unbiased estimators obtained from a quantum measurement. We quantify their performance by the usual two-sided quantum noise strain power spectral density (PSD) of the estimation error $\delta\tilde{h} = \tilde{h} - h$ [3, 19]:

$$S_h[\Omega] := \frac{\langle \{\delta\tilde{h}[\Omega], \delta\tilde{h}[\Omega]^\dagger\} \rangle}{2T} = \frac{\text{Var}(\tilde{\theta}_1) + \text{Var}(\tilde{\theta}_2)}{\|\chi[\Omega]\|^2} \quad (3)$$

For the Gaussian output states considered here, their quantum noise is fully characterized by the hermitian positive definite, spectral density matrix $\bar{S}[\Omega]$ of the output quadratures [6, 7] which we decompose as [18]

$$\begin{aligned} \bar{S}[\Omega] &:= \frac{\langle \{\delta x^{\text{out}}[\Omega], \delta x^{\text{out}}[\Omega]^\dagger\} \rangle}{2T} \\ &= R(\phi) S(r) \begin{pmatrix} \Sigma & i\Delta \\ -i\Delta & \Sigma \end{pmatrix} S(r) R(\phi)^\top. \end{aligned} \quad (4)$$

Here $R(\phi)$ is a rotation matrix, $S(r) = \text{diag}(e^r, e^{-r})$, and the real frequency-dependent parameters obey $\Sigma \geq 1/2$ and $\Sigma - |\Delta| \geq 1/2$. The parameters r, ϕ describe output-referred squeezing, while $\Sigma \pm \Delta$ are the effective thermal variances of the $\pm\Omega$ sideband modes after removing that squeezing. Thus $\Delta \neq 0$ is a sideband-noise imbalance, which drives the separation between the QCRB, HCRB, and variational readout below.

In the rest of this paper, we focus on tuned linear sensors, where the normalized response is $\chi[\Omega] \propto (0, 1)^\top$, so the signals sit entirely in the phase quadrature in the two-photon picture. Equivalently, in the single-photon picture, θ_1 (θ_2) sits (a)symmetrically in quadratures of the $\pm\Omega$ sidebands (see Fig. 1 and End Matter).

Variational readout — We first review homodyne detection and variational readout [3, 6, 20]. Homodyne detection measures an output quadrature $u^\top x^{\text{out}}[\Omega]$ with $u = (\cos \zeta, \sin \zeta)^\top$, $\zeta \in [0, 2\pi)$. Variational readout optimizes ζ at each frequency, giving (Eqs. (3) and (4))

$$S_h^{\text{var}}[\Omega] = \min_{\zeta \in [0, 2\pi)} \frac{u^\top \bar{S}[\Omega] u}{|u^\top \chi[\Omega]|^2}. \quad (5)$$

This minimization can be carried out exactly [21] and yields the closed-form expression

$$S_h^{\text{var}}[\Omega] = \frac{\Sigma}{g\|\chi\|^2} \quad (6)$$

where all parameters on the right hand side are evaluated at Ω and $g := e^{2r} \cos^2 \phi + e^{-2r} \sin^2 \phi$ is the signal gain due to the output-referred squeezing.

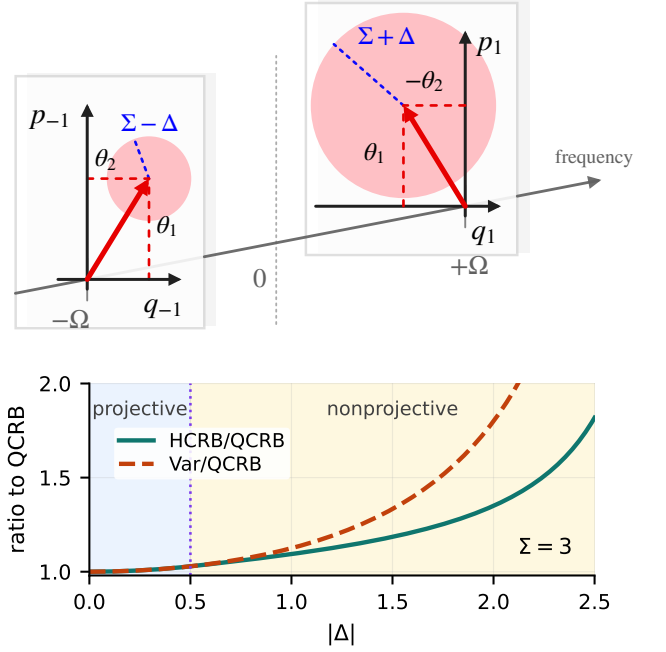


FIG. 1. *Top*: Phase space representations of the output quantum state in the sideband modes (see End Matter). For clarity, we set here $r = \phi = 0$. *Bottom*: Ratios $S_h^{\text{HCRB}}/S_h^{\text{QCRB}}$ and $S_h^{\text{var}}/S_h^{\text{QCRB}}$ as functions of $|\Delta|$ for $\Sigma = 3$. In the projective branch $0 < |\Delta| \leq 1/2$, one has $\text{Var} = \text{HCRB} > \text{QCRB}$, while in the nonprojective branch $|\Delta| > 1/2$, $\text{Var} > \text{HCRB} > \text{QCRB}$.

Quantum Cramer Rao Bound — The QCRB [7, 17] is the single-parameter quantum limit obtained by optimizing the readout separately for each component θ_i . The calculation [21] yields

$$S_h^{\text{QCRB}}[\Omega] := \frac{\Sigma^2 - \Delta^2}{g\Sigma\|\chi\|^2}. \quad (7)$$

In a multiparameter problem, however, this lower bound need not be attainable, because the individual optimal estimators $\tilde{\theta}_1^{\text{QCRB}}, \tilde{\theta}_2^{\text{QCRB}}$ (see End Matter) can be incompatible. Indeed, for lossy systems, the corresponding symmetric logarithmic derivatives do not commute in general [22, 23], even though the parameter generators do [24]. Here, they suffer from an incompatibility

$$[\tilde{\theta}_1^{\text{QCRB}}, \tilde{\theta}_2^{\text{QCRB}}] = -i \frac{\Delta}{g\Sigma}, \quad (8)$$

which does not vanish in the general $\Delta \neq 0$ case.

Holevo Cramer Rao Bound — The HCRB resolves this incompatibility issue: it minimizes the error over all jointly measurable estimators $[\tilde{\theta}_1, \tilde{\theta}_2] = 0$ and is therefore the attainable multiparameter quantum limit [23]. It takes the compact form [21]

$$S_h^{\text{HCRB}}[\Omega] := \frac{1}{g\|\chi\|^2} \left[\Sigma - \frac{(\text{ReLU}(2|\Delta| - 1))^2}{4\Sigma} \right] \quad (9)$$

where the rectified linear unit [25] is defined as $\text{ReLU}(x) := \max(x, 0)$. We call the optimum projective when it is attainable by a projective measurement (PVM) on the signal sideband modes, possibly after active Gaussian processing. We call it *nonprojective* when no PVM on the signal modes attains it, so an ancilla-assisted POVM is required, such as heterodyne detection after active Gaussian processing. As we shall see below, the ReLU term is precisely the improvement over projective strategies which is available only in that latter case: it vanishes when $|\Delta| \leq 1/2$ and activates when $|\Delta| > 1/2$ to lower the HCRB (see Table I).

Comparing Eqs. (7) and (9), one has $S_h^{\text{QCRB}} \leq S_h^{\text{HCRB}}$, with equality only for $\Delta = 0$. Physically, $\Delta \neq 0$ means that the two sidebands are unequally noisy. The separate QCRB estimators weight the cleaner sideband more strongly. Since that same sideband carries θ_1 and θ_2 in conjugate quadratures, these separate optima are not jointly measurable.

The HCRB is then the best joint compromise. For $0 < |\Delta| \leq 1/2$, the optimum remains projective and coincides with variational readout, $S_h^{\text{HCRB}} = S_h^{\text{var}}$. For $|\Delta| > 1/2$, an ancilla-assisted POVM becomes advantageous and $S_h^{\text{QCRB}} < S_h^{\text{HCRB}} < S_h^{\text{var}}$. In the extreme imbalance limit $\Sigma \rightarrow \infty$, $|\Delta| \rightarrow \Sigma - 1/2$, the HCRB tends to the universal bound of twice the QCRB [26, 27]. Fig. 1 illustrates this hierarchy for $\Sigma = 3$.

Attainability of the HCRB — For Gaussian shift models, the HCRB (Eq. (9)) is not only a bound: it is exactly attainable by a suitable Gaussian measurement on the single-copy level, so it gives the tight spectral limit [22, 23]. We now identify the ideal broadband measurement that attains it, and then a narrowband implementation requiring only a modulated local oscillator.

In the projective regime ($|\Delta| \leq 1/2$), we have already seen that variational readout followed by sine/cosine demodulation to construct $\tilde{h}[\Omega]$ is optimal. In the nonprojective regime ($|\Delta| > 1/2$), the optimal measurement corresponds to a *variational Gaussian processing* built from frequency-dependent squeezers, followed by heterodyne detection [21] (see Fig. 2(b) for illustration using a single squeezer). Because $\Delta[\Omega]$ can cross the projective/nonprojective threshold as a function of frequency, an ideal broadband implementation would first spatially separate the two regimes, for example with a Fabry–Perot spectral demultiplexer.

A simpler narrowband route is *symplectodyne* readout: balanced detection with a two-tone local oscillator (LO), followed by classical post-processing of the photocurrent harmonics (see Fig. 2(c-d)). This synthesizes the same effective squeezed-heterodyne statistic without requiring a physical squeezer. The signal-free image sidebands supply the vacuum ancilla required by the optimal POVM. Adding more tones in the LO gives no broadband advantage [21].

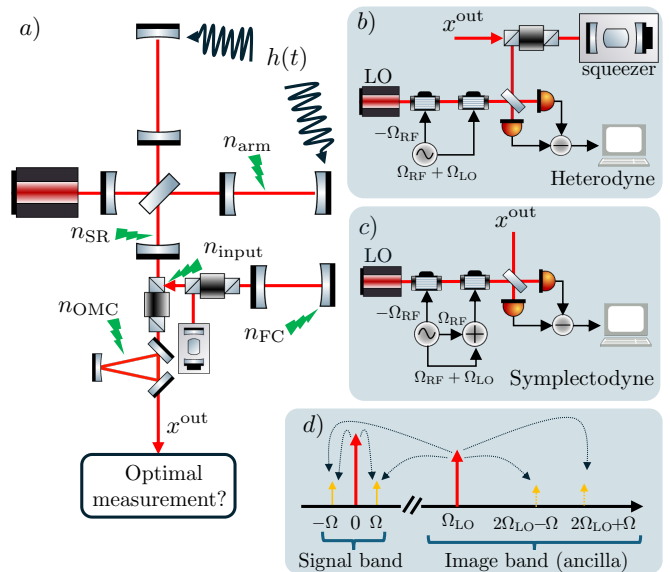


FIG. 2. (a) Simplified scheme of LIGO with frequency-dependent squeezing and examples of realistic losses (Filter cavity n_{FC} , dark port input n_{input} , signal recycling cavity n_{SR} , arm cavities n_{arm} , output mode cleaner n_{OMC}). (b) HCRB-optimal POVM: the output undergoes Gaussian processing (squeezer), then is detected using heterodyne at frequency Ω_{LO} outside of the signal band (\sim MHz for LIGO). (c,d) Symplectodyne readout: a three-channel RF generator, combined with a pair of upshift/downshift Acousto-Optic Modulators, creates a two-tone local oscillator (carrier frequency and sideband Ω_{LO}); physical Gaussian processing is avoided and image-band ancilla modes are automatically included.

Application to LIGO O4 — We now apply the theory to the measured LIGO quantum-noise budget in O4, taken from [14]. In Eq. (1), x^{in} is the injected squeezed vacuum, and the n_j are vacuum modes describing optical losses at different points of the propagation through the interferometer [12] (see Fig. 2 (a) for a visual representation of the interferometer and some of the loss terms). We obtain H, T_j, χ (which include mode mismatch effects) at each frequency using the `gwinc` Python package [28], then extract r, ϕ, Σ, Δ from Eq. (4). Phase noise is incorporated in these parameters as described in [21]. Although the signal extraction cavity is slightly detuned [14, 15], the response is well approximated by the tuned condition $\chi \propto (0, 1)^{\text{T}}$ so that our general closed-form expressions can be applied [21]. In all comparisons below, the interferometer and squeezing parameters are fixed to the O4 configuration; only the readout is varied for a fair comparison.

The extracted imbalance crosses the nonprojective threshold, $|\Delta(\Omega)| > 1/2$, from 12 Hz to 74 Hz (Fig. 3). In this band the Homodyne-HCRB-QCRB hierarchy is strict, with peak PSD ratios $\max(S_h^{\text{HCRB}}/S_h^{\text{QCRB}}) \approx 1.3$ and $\max(S_h^{\text{var}}/S_h^{\text{QCRB}}) \approx 1.6$. The imbalance is driven by the combination of high generated squeezing (17 dB,

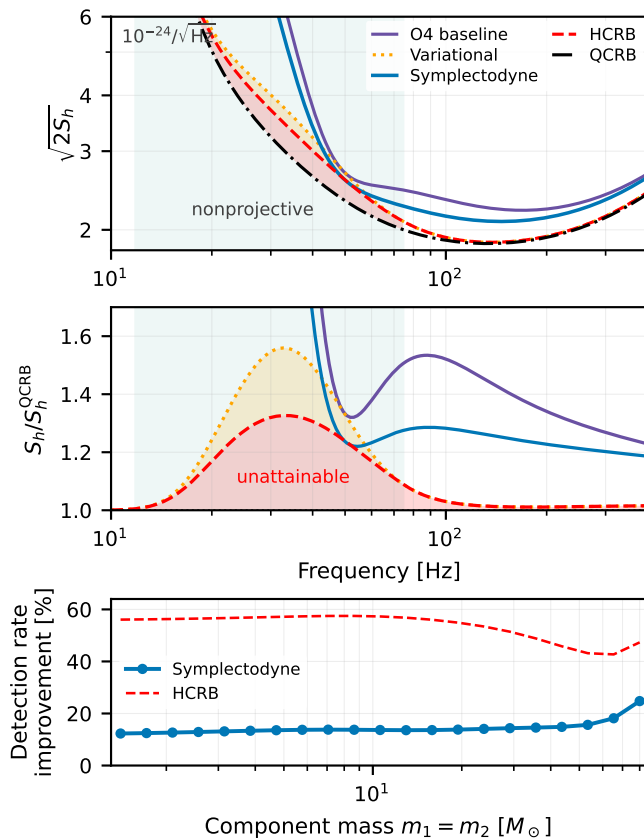


FIG. 3. LIGO O4 quantum-noise hierarchy and astrophysical impact. *Top*: One-sided quantum strain amplitude spectral density, for baseline LIGO O4, variational readout, symplectodyne optimized at 50 Hz, HCRB, and QCRB. *Middle*: PSD ratios to the QCRB; yellow fills mark the region where symplectodyne has an advantage over homodyne; red fill marks the unattainable QCRB–HCRB gap. *Bottom*: Relative detection-rate improvement over baseline O4 for equal-mass binaries, using the full O4 classical plus quantum noise budget, with the optimal symplectodyne readout or the HCRB noise floor.

compared to 6 dB measured at the output) and filter-cavity detuning mismatch, which rotates and dephases the squeezed field near the 26 Hz filter-cavity detuning [12, 13, 18, 29, 30].

We also show, in the top and middle plots of Fig. 3, the broadband performance of a symplectodyne readout optimized to reach the HCRB at 50 Hz, which outperforms variational readout in the 43 – 57 Hz band, and outperforms the homodyne-type O4 readout [15, 31, 32] over the whole detection band. Its practical advantage is that the required operation is transferred to the local oscillator: no additional optical element is inserted in the signal path, so the output field is not exposed to extra readout loss. By contrast, broadband variational readout and variational Gaussian processing require low-loss kilometer-scale output filter cavities and squeezers in the signal path, making its performance highly sensitive to

optical loss [3].

As a simple astrophysical figure of merit, we add the standard O4 classical noise budget (seismic, thermal, residual gas, etc.) to the quantum noise spectrum and convert into inspiral range and hence detection rate for equal-mass compact binaries. Fig. 3 (bottom plot) summarizes the improvements in detection rate relative to the baseline LIGO O4 configuration for equal mass compact binary mergers. With the full O4 classical and quantum noise budget, optimized symplectodynes for each component mass provide a 12–25% improvement compared to the homodyne-type readout experimentally implemented in LIGO O4, while the HCRB sets a 43–57% ceiling for the same baseline. An adaptive symplectodyne readout could reach this ceiling in the adiabatic limit, by tuning the LO modulation across the instantaneous frequency trace of the chirped signal.

The symplectodyne gain is largest for the heaviest binaries, which weight the nonprojective band most strongly. This mass range is astrophysically motivated: binaries with component masses $\gtrsim 50 M_\odot$ probe the onset of the pair-instability regime and likely hierarchical mergers, while events such as GW190521 already show that they can produce intermediate-mass-black-hole remnants [33–35]. Thus improved low-frequency quantum readouts are especially relevant for formation-channel studies and black-hole spectroscopy [35, 36].

Conclusion — In this Letter, we developed a general framework for Gaussian quantum waveform estimation in tuned linear sensors with realistic degradation. The result is a compact closed-form hierarchy for variational readout, the QCRB, and the attainable HCRB, that arises only when sideband imbalance is properly considered. This imbalance, missed by the previous simplified models [7, 8, 37], is what separates the ideal single-parameter QCRB from the true multiparameter quantum limit even when the sensor is tuned.

Applying the framework to the LIGO O4 quantum-noise budget, we found that the detector already operates in a nonprojective band where $S_h^{\text{QCRB}} < S_h^{\text{HCRB}} < S_h^{\text{var}}$. The optimal readout is therefore not ordinary homodyne detection, but an ancilla-assisted Gaussian measurement. Our symplectodyne construction realizes this measurement narrowband by shaping the local oscillator rather than inserting lossy optics in the signal path. Additionally, unlike synodyne detection [38, 39], which causes frequency folding and downconversion to noise-prone low frequencies, symplectodyne places its auxiliary tones outside the GW band. This makes it a natural candidate for future upgrades and next-generation detectors [15, 40, 41], where larger generated squeezing and lower classical noise should increase the advantage of mitigating dephasing noise and accessing the HCRB.

In our analysis, we fixed the input squeezed state and optimized the measurement. A complementary state-preparation approach is to adjust the input squeezing

level to decrease dephasing noise; this can also lead to an enhancement in detection rate [21], but changes the quantum statistical model and therefore the relevant quantum Cramer–Rao and Holevo bounds. The advantage of symplectodyne detection compared to squeezing input optimization is that the local oscillator is RF-modulated electronically, while the bandwidths of the filter cavity and the interferometer are limited by the kHz-band signal frequencies. Thus symplectodyne can in principle be controlled much faster, which may enable adaptive readout after early warning of gravitational-wave signals.

Beyond gravitational-wave interferometry, our derivation gives a rare analytic example of an attainable multiparameter quantum bound for a mixed-state Gaussian model. General HCRB calculations usually require optimizing over density-operator geometry or solving semidefinite programs [23, 42, 43], which may obscure the intuition of the underlying physical mechanisms. Here the conjugate-symplectic reduction of Eq. (4) turns the problem into elementary matrix algebra, making the role of sideband imbalance and measurement incompatibility explicit. In this Gaussian-shift setting, we note that the HCRB also coincides with the most-informative bound [44, 45].

Future work should quantify technical noise from LO modulation, and explore whether non-Gaussian input states, which can reduce incompatibility in joint quadrature-displacement estimation [46, 47], can further improve the attainable waveform limit. Astrophysical figures of merit other than the inspiral range, such as parameter-estimation accuracy, early-warning time, or population-dependent rates, may also lead to different optimal quantum schemes.

Acknowledgments We thank Lee McCuller for useful comments regarding the manuscript. We thank Wenxuan Jia & Kevin Kuns for insightful discussions regarding the GWINC Python package and the LIGO O4 noise budget. We acknowledge helpful contributions from OpenAI GPT 5.2 & 5.4 on the derivations of the HCRB (Eq. (9)) and the optimality of the symplectodyne readout. The authors are fully responsible for the scientific content and integrity of this work. J.W.G. acknowledges support from the ARO (W911NF-23-1-0077), ARO MURI (W911NF-21-1-0325), AFOSR MURI (FA9550-21-1-0209, FA9550-23-1-0338), DARPA (HR0011-24-9-0359, HR0011-24-9-0361), NSF (ERC-1941583, OMA-2137642, OSI-2326767, CCF-2312755, OSI-2426975), Packard Foundation (2020-71479), and DOE (DE-AC02-06CH11357). T.G. acknowledges funding from ISF Grant No. 3302/25, and the quantum science and technology early-career grant of the Israeli council for higher education. Y.C. acknowledges support from the Simons Foundation (Award No. 568762) and the National Science Foundation (via Grants No. PHY-2309211 and No. PHY-2309231).

-
- * ding@apc.in2p3.fr
- [1] C. W. Helstrom, *Journal of Statistical Physics* **1**, 231 (1969).
 - [2] C. W. Helstrom, *Quantum Detection and Estimation Theory* (Academic Press, New York, 1976).
 - [3] H. J. Kimble, Y. Levin, A. B. Matsko, K. S. Thorne, and S. P. Vyatchanin, *Phys. Rev. D* **65**, 022002 (2001).
 - [4] A. Buonanno and Y. Chen, *Physical Review D* **64**, 10.1103/physrevd.64.042006 (2001).
 - [5] A. Buonanno and Y. Chen, *Physical Review D* **65**, 10.1103/physrevd.65.042001 (2002).
 - [6] S. L. Danilishin and F. Y. Khalili, *Living Reviews in Relativity* **15**, 5 (2012).
 - [7] H. Miao, R. X. Adhikari, Y. Ma, B. Pang, and Y. Chen, *Physical Review Letters* **119**, 10.1103/physrevlett.119.050801 (2017).
 - [8] J. W. Gardner, T. Gefen, S. A. Haine, J. J. Hope, and Y. Chen, *Physical Review Letters* **132**, 130801 (2024).
 - [9] T. Gefen, R. Tarafder, R. X. Adhikari, and Y. Chen, *Phys. Rev. Lett.* **132**, 020801 (2024).
 - [10] D. Ganapathy, W. Jia, M. Nakano, V. Xu, N. Aritomi, T. Cullen, N. Kijbunchoo, S. Dwyer, A. Mullavey, L. McCuller, and LIGO O4 Detector Collaboration, *Physical Review X* **13**, 041021 (2023).
 - [11] F. Acernese *et al.* (Virgo Collaboration), *Phys. Rev. Lett.* **131**, 041403 (2023).
 - [12] P. Kwee, J. Miller, T. Isogai, L. Barsotti, and M. Evans, *Phys. Rev. D* **90**, 062006 (2014).
 - [13] L. McCuller, S. E. Dwyer, A. C. Green, H. Yu, K. Kuns, *et al.*, *Phys. Rev. D* **104**, 062006 (2021).
 - [14] W. Jia, V. Xu, K. Kuns, M. Nakano, L. Barsotti, M. Evans, N. Mavalvala, and members of the LIGO Scientific Collaboration, *Science* **385**, 1318 (2024).
 - [15] E. Capote *et al.* (LIGO O4 Detector Collaboration), *Physical Review D* **111**, 10.1103/physrevd.111.062002 (2025).
 - [16] C. W. Gardiner and P. Zoller, *Quantum Noise* (Springer, 1999).
 - [17] H. Miao, *Physical Review A* **95**, 10.1103/physreva.95.012103 (2017).
 - [18] J. Ding, H. A. Loughlin, and V. Sudhir, *Quantum linear time-translation-invariant systems: Conjugate symplectic structure, uncertainty bounds, and tomography* (2024), arXiv:2410.09976 [quant-ph].
 - [19] M. Maggiore, *Gravitational Waves. Volume 1: Theory and Experiments* (Oxford University Press, Oxford, 2008).
 - [20] S. P. Vyatchanin and E. A. Zubova, *Physics Letters A* **201**, 269 (1995).
 - [21] See Supplemental Material for derivations of the variational, QCRB, and HCRB spectra, details of the optimal Gaussian and symplectodyne measurements, and numerical validation of the LIGO O4 application.
 - [22] R. Demkowicz-Dobrzański, W. Górecki, and M. Guţă, *Journal of Physics A: Mathematical and Theoretical* **53**, 363001 (2020).
 - [23] A. Holevo, *Probabilistic and Statistical Aspects of Quantum Theory*, 1st ed., Publications of the Scuola Normale Superiore, Vol. 1 (Edizioni della Normale, Pisa, 2011).
 - [24] S. Imai, J. Yang, and L. Pezzè, *Hierarchy of saturation conditions for multiparameter quantum metrology*

- bounds (2026), arXiv:2602.12097 [quant-ph].
- [25] F. Bach, *Learning Theory from First Principles* (The MIT Press, 2024).
- [26] A. Carollo, B. Spagnolo, A. A. Dubkov, and D. Valenti, *Journal of Statistical Mechanics: Theory and Experiment* **2019**, 094010 (2019).
- [27] M. Tsang, F. Albarelli, and A. Datta, *Physical Review X* **10**, 031023 (2020).
- [28] J. G. Rollins, E. Hall, C. Wipf, and L. McCuller, *pygwinc: Gravitational wave interferometer noise calculator*, *Astrophysics Source Code Library*, record ascl:2007.020 (2020).
- [29] S. Grebien, J. Gurs, R. Schnabel, and M. Korobko, *Hyperloss from coherent spatial-mode mixing in quantum-correlated networks* (2026), arXiv:2603.21982 [quant-ph].
- [30] K. Kuns and D. Brown, *Squeezed state degradations due to mode mismatch and thermal aberrations in gravitational wave detectors* (2026), LIGO-P2500132, CEP2400005, arXiv:2604.23835 [physics.ins-det].
- [31] S. Hild, H. Grote, J. Degallaix, S. Chelkowski, K. Danzmann, A. Freise, M. Hewitson, J. Hough, H. Lück, M. Prijatelj, K. A. Strain, J. R. Smith, and B. Willke, *Classical and Quantum Gravity* **26**, 055012 (2009).
- [32] T. T. Fricke, N. D. Smith-Lefebvre, R. Abbott, R. X. Adhikari, K. L. Dooley, M. Evans, P. Fritschel, V. V. Frolov, K. Kawabe, J. S. Kissel, B. J. J. Slagmolen, and S. J. Waldman, *Classical and Quantum Gravity* **29**, 065005 (2012).
- [33] R. Abbott *et al.*, *Physical Review Letters* **125**, 10.1103/PhysRevLett.125.101102 (2020).
- [34] H. Tong, M. Fishbach, E. Thrane, *et al.*, *Nature* 10.1038/s41586-026-10359-0 (2026).
- [35] S. Torniamenti, M. Mapelli, C. Pérois, M. Arca Sedda, M. C. Artale, M. Dall'Amico, and M. P. Vaccaro, *Astronomy & Astrophysics* **688**, A148 (2024).
- [36] G. Carullo, *General Relativity and Gravitation* **57**, 76 (2025).
- [37] H. Miao, N. D. Smith, and M. Evans, *Physical Review X* **9**, 10.1103/physrevx.9.011053 (2019).
- [38] L. Buchmann, S. Schreppler, J. Kohler, N. Spethmann, and D. Stamper-Kurn, *Physical Review Letters* **117**, 030801 (2016).
- [39] C. Ockeloen-Korppi, E. Damskägg, G. Paraoanu, F. Masel, and M. Sillanpää, *Physical Review Letters* **121**, 243601 (2018).
- [40] V. Srivastava, D. Davis, K. Kuns, P. Landry, S. Ballmer, M. Evans, E. D. Hall, J. Read, and B. S. Sathyaprakash, *Science-driven tunable design of cosmic explorer detectors* (2022), arXiv:2201.10668 [gr-qc].
- [41] M. Branchesi, M. Maggiore, D. Alonso, C. Badger, B. Banerjee, F. Beirnaert, E. Belgacem, *et al.*, *Journal of Cosmology and Astroparticle Physics* **2023** (07), 068.
- [42] F. Albarelli, J. F. Friel, and A. Datta, *Physical Review Letters* **123**, 200503 (2019).
- [43] J. S. Sidhu, Y. Ouyang, E. T. Campbell, and P. Kok, *Physical Review X* **11**, 011028 (2021).
- [44] L. O. Conlon, J. Suzuki, P. K. Lam, and S. M. Assad, *Physics Letters A* **542**, 130445 (2025).
- [45] S. K. Yung, C. M. Yung, L. O. Conlon, and S. M. Assad, *The most informative cramer-rao bound for quantum two-parameter estimation with pure state probes* (2025), arXiv:2511.14950 [quant-ph].
- [46] M. Frigerio, M. G. A. Paris, C. E. Lopetegui, and M. Walschaers, *Joint estimation of position and momentum with arbitrarily high precision using non-Gaussian states* (2025), arXiv:2504.01910 [quant-ph].
- [47] L. Labarca, S. Turcotte, A. Blais, and B. Royer, *PRX Quantum* **7**, 020301 (2026).

END MATTER

Two-photon and sideband conventions

The physical sideband (or single-photon picture) modes at $\pm\Omega$ have annihilation operators $a[\pm\Omega]$ satisfying $[a[\Omega], a[\Omega']^\dagger] = 2\pi\delta[\Omega - \Omega']$. For a finite measurement time $T \simeq 2\pi\delta[0]$, we regularize these continuous-frequency modes by the bins $a_{\pm 1} = a[\pm\Omega]/\sqrt{T}$, thus satisfying $[a_m, a_n^\dagger] = \delta_{mn}$ ($m, n = \pm 1$). The quadrature vector $\mathbf{R} = (q_{+1}, p_{+1}, q_{-1}, p_{-1})^\top$ is such that

$$q_{\pm 1} = \frac{a_{\pm 1} + a_{\pm 1}^\dagger}{\sqrt{2}}, \quad p_{\pm 1} = \frac{a_{\pm 1} - a_{\pm 1}^\dagger}{i\sqrt{2}}. \quad (10)$$

In the frequency-domain input-output relation of Eq. (1), we introduce the two-photon quadratures $x[\Omega] = (q[\Omega], p[\Omega])^\top$. They are defined as

$$q[\Omega] = \frac{a[\Omega] + a^\dagger[-\Omega]}{\sqrt{2}}, \quad p[\Omega] = \frac{a[\Omega] - a^\dagger[-\Omega]}{i\sqrt{2}}. \quad (11)$$

They are not Hermitian, but obey $q[\Omega] = q[-\Omega]^\dagger$ and $p[\Omega] = p[-\Omega]^\dagger$. One has the exact conversion

$$\mathbf{R} = \frac{1}{\sqrt{T}} \begin{pmatrix} 1 & 0 & 0 & -1 \\ 0 & 1 & 1 & 0 \\ 1 & 0 & 0 & 1 \\ 0 & 1 & -1 & 0 \end{pmatrix} \begin{pmatrix} \text{Re } q[\Omega] \\ \text{Re } p[\Omega] \\ \text{Im } q[\Omega] \\ \text{Im } p[\Omega] \end{pmatrix}. \quad (12)$$

Thus the conjugate-symplectic Williamson form of \bar{S} in Eq. (4) is equivalently the ordinary 4×4 real Williamson form

$$V_R = S_R(r, \phi) \text{diag}(\Sigma + \Delta, \Sigma + \Delta, \Sigma - \Delta, \Sigma - \Delta) S_R(r, \phi)^\top, \quad (13)$$

where $V_R = \langle \{\delta \mathbf{R}, \delta \mathbf{R}^\top\} \rangle / 2$ and

$$S_R(r, \phi) = \begin{pmatrix} \cosh r & 0 & \sinh r \cos(2\phi) & \sinh r \sin(2\phi) \\ 0 & \cosh r & \sinh r \sin(2\phi) & -\sinh r \cos(2\phi) \\ \sinh r \cos(2\phi) & \sinh r \sin(2\phi) & \cosh r & 0 \\ \sinh r \sin(2\phi) & -\sinh r \cos(2\phi) & 0 & \cosh r \end{pmatrix} \quad (14)$$

is a rotated two-mode squeezing matrix.

When $\chi / \|\chi\| = (0, 1)^\top$, as assumed in this Letter, the mean displacement on the sideband modes is

$$\langle \mathbf{R} \rangle = (-\theta_2, \theta_1, \theta_2, \theta_1)^\top. \quad (15)$$

The top panel of Fig. 1 is the $r = \phi = 0$ version of this representation: the $+\Omega$ and $-\Omega$ sideband modes have thermal variances $\Sigma + \Delta$ and $\Sigma - \Delta$, respectively, while θ_1 displaces both phase quadratures and θ_2 displaces the two amplitude quadratures with opposite signs.

Optimal estimators

The optimal estimators for variational readout, QCRB, and HCRB are given by

$$\tilde{\theta}_1^\bullet + i\tilde{\theta}_2^\bullet = u_\bullet^\dagger x^{\text{out}}[\Omega] + \nu_\bullet, \quad \bullet \in \{\text{var}, \text{QCRB}, \text{HCRB}\}, \quad (16)$$

where

$$u_{\text{var}}^\dagger = \frac{1}{\sqrt{T}} \left(\frac{(e^{-2r} - e^{2r}) \sin(2\phi)}{2g}, 1 \right), \quad \nu_{\text{var}} = 0, \quad (17)$$

$$u_{\text{QCRB}}^\dagger = \frac{1}{\sqrt{T}} \left(\frac{(e^{-2r} - e^{2r}) \sin(2\phi)}{2g} + i \frac{\Delta}{g\Sigma}, 1 \right), \quad \nu_{\text{QCRB}} = 0, \quad (18)$$

$$u_{\text{HCRB}}^\dagger = \frac{1}{\sqrt{T}} \left(\frac{(e^{-2r} - e^{2r}) \sin(2\phi)}{2g} + i \frac{\text{sgn}(\Delta) \text{ReLU}(2|\Delta| - 1)}{2g\Sigma}, 1 \right), \quad \nu_{\text{HCRB}} = \sqrt{\frac{\text{ReLU}(2|\Delta| - 1)}{2g\Sigma}} [-\text{sgn}(\Delta)p_a + iq_a]. \quad (19)$$

Here $a_a = (q_a + ip_a)/\sqrt{2}$ is an independent vacuum ancilla mode, with $[q_a, p_a] = i$ and $\text{Var}(q_a) = \text{Var}(p_a) = 1/2$.